

Electroless Synthesis of Ag Nanoparticles on Deposited Nanostructured Si Films

A. Kaan Kalkan* and Stephen J. Fonash

Center for Nanotechnology Education and Utilization, The Pennsylvania State University,
University Park, Pennsylvania 16802

Received: June 3, 2005; In Final Form: August 26, 2005

Two and three-dimensional Ag nanoparticle ensembles were synthesized on deposited nanostructured column-void Si films simply by film immersion into pure Ag_2SO_4 or AgNO_3 solutions. In addition to functioning as a reducer, this nanostructured material provides immobilization and monodispersion of the Ag nanoparticles due to its systematic nanoscale topography. This is accomplished without the requirement of a surfactant, capping agent, or linker. Kinetics, as monitored from plasmon optical extinction, and infrared spectroscopy suggest accompanying oxide growth limits and finally inhibits synthesis enabling nanoparticle size control. Kinetics is also limited by Ag^+ transport through the voids unless the Si film is ultrathin. Our synthesis approach offers significant advantages for surface-enhanced molecular detection, including the absence of any agents on the nanoparticle surfaces and the ability to obtain nanoparticle ensembles on any substrate.

Introduction

There is growing interest in analytical techniques employing noble metal nanoparticles. This activity is being stimulated by the ultrasensitive detection achieved in characterization approaches based on surface-enhanced optical phenomena, such as surface-enhanced Raman scattering (SERS),^{1,2} surface plasmon resonance,³ and surface-enhanced fluorescence.⁴ All of these surface-enhanced optical phenomena are attributable to the local concentration of electromagnetic fields that occur in the close vicinity of optically excited metallic nanostructures.⁵ These intense near fields develop as a result of their resonant coupling with the collective electron oscillations (localized surface plasmon modes) of the nanoparticles.⁵ Such enhanced characterization approaches would be most versatile and very amenable to high-throughput if the required ensembles of nanoparticles were positioned on solid substrates, on which analyte samples could then be spotted and analyzed in minutes. As a result of this need, methods to synthesize noble nanoparticles immobilized on surfaces and with controlled size and spacing have been the subject of extensive exploration in recent years.^{1–11} Several “bottom-up” and self-assembling approaches have been recently demonstrated for fabricating such ensembles.^{1,3,6–11} The majority of these approaches are based on transfer of solution-phase-synthesized particles onto substrate surfaces by processes such as immersion and spin coating,^{1,6–8} the Langmuir–Blodgett technique,⁹ or electrophoretic positioning.¹⁰ The particles are then anchored to the substrates by electrostatic attraction,^{1,6} hydrogen bonds,⁶ or covalent linkers.^{7,8} Alternatively, direct synthesis of such nanoparticles onto substrates has been achieved, for example, by photothermal reduction of metal precursors in mesoporous template films,¹¹ or by a combination of vapor deposition with nanosphere lithography.³

We report here on a new approach to synthesizing two-dimensional (2D) or three-dimensional (3D) ensembles of immobilized and monodispersed, size-controlled Ag nanoparticles using a deposited nanostructured film. This enabling

deposited material is column-void (c-v) silicon, which we have reported on elsewhere.^{12,13} The nanoparticle synthesis occurs by simply exposing these nanostructured Si films to pure Ag_2SO_4 or AgNO_3 solutions at room temperature. We attribute the nanoparticle synthesis to reduction of Ag^+ by the nanostructured Si. These same solutions do not lead to Ag nanoparticle formation on flat Si surfaces.¹⁴ As shown by Ohmi et al.,¹⁵ the reduction of noble metal cations occurs on flat Si surfaces, but it is only observed at contamination levels. In this situation, reduction is probably terminated before stable metal nanoparticles can form due to the hindrance of essential charge transfer by a surface oxide forming in parallel with reduction. However, electroless nanoparticle deposition does occur on flat Si surfaces in noble metal salt solutions, if HF is introduced.^{14,16,17} Flat Ge surfaces have also been found to support electroless growth of noble metal nanoparticles using pure aqueous metal salt solutions without HF.¹⁸ The effect of HF in the case of flat Si is easily understood due to its role in silicon oxide etching and, in the case of Ge, it is well-known that Ge oxide dissolves in water.¹⁸

In addition to our results reported here, the ability of nanostructured Si to support electroless deposition, without the need for HF, has been observed for free-standing Si nanowires grown from the vapor phase¹⁹ and for electrochemically etched mesoporous Si.²⁰ However, particle size control as a result of the self-limiting feature of the synthesis and monodispersion of particles were not demonstrated for either of these cases nor were kinetics studies undertaken. In this article we report on the unique features of Ag nanoparticle growth on our c-v deposited silicon including the self-limiting kinetics, which enables particle size control, and the particle monodispersion and immobilization due to the nanotopography of the Si films.

Experimental Details

The specifics of the deposition of the nanostructured c-v Si films employed in the present work are listed in Table 1. As described in detail elsewhere,^{12,13,21} our high-density plasma deposition process brings together the extreme conditions of low substrate temperature, reduced ion bombardment, and highly

* Address correspondence to this author. E-mail: akk105@psu.edu.

TABLE 1: Nanostructured Column-Void Si Film Deposition Process Details

deposition system	PlasmaTherm SLR 770 ECR-PECVD
upper magnet current	173 A
lower magnet current	24 A
substrate temperature	100 °C
incident microwave power	400 W
reflected microwave power	20–40 W
process pressure	10 mTorr
SiH ₄ flow rate	1.5 sccm
SiF ₄ flow rate	0.4 sccm
H ₂ flow rate	40 sccm
deposition rate	~20 nm/min
substrate	Corning 1737 glass, 0.7 mm thick (unless otherwise stated)

reactive deposition species. The consequence is low adatom mobility accounting for ballistic-like features of the deposition leading to pronounced self-shadowing and thereby to a nanoscale column-void structure. While the synthesis of Ag nanoparticles already occurs using our c-v Si films grown without SiF₄, the incorporation of SiF₄ in addition to SiH₄ as the precursor gas was found to enhance columnar separation and to prevent columnar aggregation.¹³ Hence, as seen in Table 1, SiF₄ was employed for these c-v Si films to enhance accessible inner surface area and subsequent Ag nanoparticle density.

The nanoparticles of this study were then grown by immersion of the c-v Si films into solutions of Ag₂SO₄ or AgNO₃ (metal salts were purchased from Aldrich at 99.999% purity and then dissolved in deionized water). The size and dispersion of the resulting Ag nanoparticles grown on these c-v Si films were explored with a field emission scanning electron microscope (Leo 1530) at the electron energy of 2 keV. An FEI/Philips 420ST transmission electron microscope equipped with a Gresham Sirius 30 Si (Li) X-ray detector (for energy-dispersive X-ray spectroscopy (EDS)) was employed (120 keV) to investigate the shape and composition/structure of the Ag nanoparticles.

The kinetics of the Ag nanoparticle synthesis was studied via optical extinction measured by a Cary 300 spectrophotometer. Optical extinction of the Ag nanoparticles was derived by subtracting the absorbance ($-\log(\text{transmission})$) of unexposed Si film (without Ag nanoparticles) from that of immersed film (with nanoparticles). In particular, for the in situ kinetics measurements, we placed the Si films (deposited on 8 mm × 25 mm Corning 1737 glass) in a standard quartz cell holder and then subjected them to immersion with 3 mL of AgNO₃ solution. The surface chemistry changes during particle growth were monitored with a BIO-RAD Fourier transform infrared (FTIR) spectrometer. For this study, the c-v Si films were deposited on double side polished oxygen-free undoped flat-zone-grown Si wafers.

Results and Discussion

As seen in Figure 1, our c-v Si film material utilized in this work has a systematic topography composed of 20–30 nm wide nanocolumns with an average separation of 20 nm. As we have established previously, the building blocks of the nanocolumns are Si nanocrystals accounting for undulations on the surface of Si columns.^{12,13} It is likely that the enhanced electric fields at such high curvature features facilitate the charge transport through the oxide layer during Ag reduction permitting the formation of stable nanoparticles without the need for oxide removal by HF. Figure 2 depicts the time evolution of the optical extinction resulting from Ag nanoparticle growth for a c-v Si film immersed in a 0.001 M Ag₂SO₄ solution. The extinction

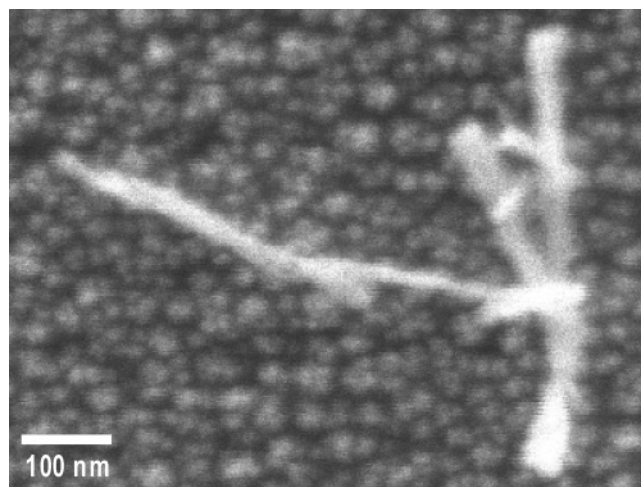


Figure 1. Plan (SEM) view of a nanostructured c-v Si film. The film was grown as described in Table 1 on a glass substrate to a thickness of about 400 nm. Several nanocolumns detached from the substrate and lying on the film surface are seen.

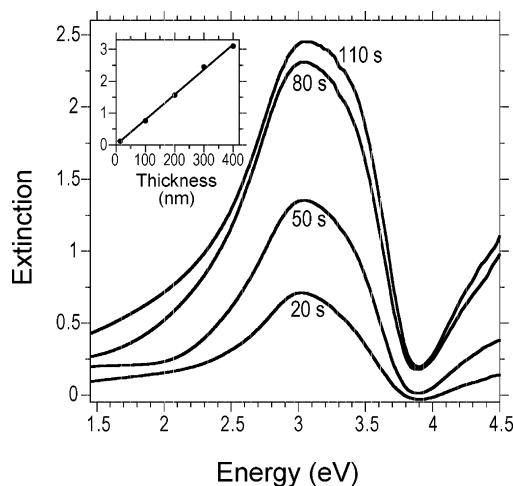


Figure 2. Time evolution of the optical extinction associated with growing Ag nanoparticles resulting from the immersion of a 300 nm thick c-v Si film into 0.001 M Ag₂SO₄ solution. The solution was contained in a 400 mL beaker held at 20 °C and stirred at 20 rpm during synthesis. Inset: intensity of saturated plasmon extinction (at 3.05 eV) as a function of Si film thickness (0.002 M Ag⁺, 20 °C).

band peaking at 3.05 eV is characteristic of the particle plasmon resonance associated with spherical Ag nanoparticles.⁵ A monotonic increase in optical extinction is seen up to ~80 s, beyond which it slows down and completely saturates at ~90 s, indicative of no further Ag nanoparticle growth. The saturated intensity of plasmon optical extinction is found to increase linearly with the Si film thickness, as shown in the inset of Figure 2 (at 3.05 eV). Hence, we infer the Ag particles are synthesized throughout the thickness (i.e., void network) of the Si film in a 3D ensemble fashion.

With the objective of studying the size and dispersion of the nanoparticles by scanning electron microscopy (SEM), we removed a film with synthesized nanoparticles from its glass substrate and transferred it to an adhesive SEM carbon pad. In Figure 3a flakes of this Si film with synthesized Ag nanoparticles (brighter tone) are seen providing us with a plan (right) and several cross sectional (left) views of the film layer. For this particular case, the film had been immersed in 0.002 M AgNO₃ for 90 s. In agreement with the optical extinction data, the void network of the Si film is seen to be infused with Ag

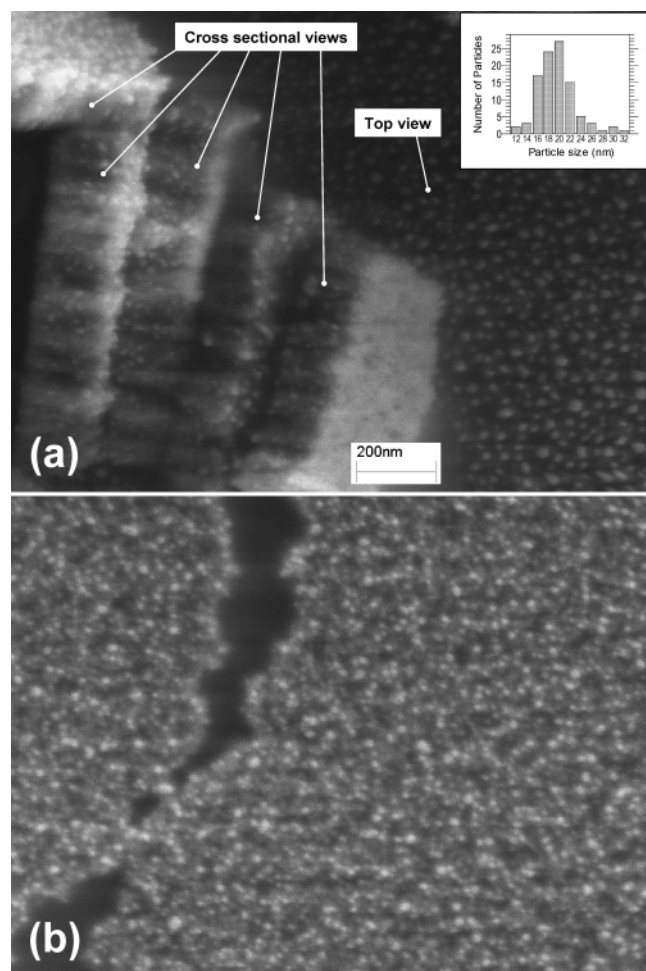


Figure 3. SEM micrographs showing flakes of a nanostructured c-v Si film (200 nm thick) lifted off from its glass substrate and subsequently transferred onto a SEM carbon pad. Prior to the lift-off, the film was immersed in 0.002 M AgNO_3 for 90 s with 20 rpm stirring at 20 °C. Ag nanoparticles synthesized are seen in brighter tone. (a) Top and cross sectional views (several flakes tilted up—see left side). The inset shows the size distribution corresponding to 100 adjacent particles situated at the right bottom corner (top view). The size labels of the horizontal axis correspond to 2 nm size intervals. For instance, 20 nm covers all particles in the size range between 19 and 21 nm. (b) Bottom view, flakes turned upside down.

nanoparticles throughout its cross section. In fact, Figure 3b shows the film layer from the bottom view; i.e., it shows flakes turned upside down. As seen, the Ag particle growth occurs even at the bottom of the c-v Si film. The embedded particles at the bottom are observed to be somewhat smaller than the ones on the top surface of the c-v Si film with average sizes of 16 and 20 nm, respectively. The plan view also reveals that the particles are dispersed on the top surface of the Si film with an average center-to-center distance of 50 nm. This corresponds to the average center-to-center distance of the Si columns. Hence, the dispersion of the particles is seen to follow the systematically varying topography features of the c-v Si. The inset of Figure 3a shows the size distribution corresponding to 100 adjacent particles on the top surface (sampled from the right bottom corner of the figure).

Figure 4a shows a representative TEM image of a Si nanocolumn detached from glass substrate after Ag nanoparticle synthesis (0.002 M AgNO_3 , 90 s, 20 rpm stirring). The diameter of the Si column coated with Ag nanoparticles is seen to be about 60 nm. We infer that the column diameter was about 30 nm before nanoparticle synthesis, since the sizes of the

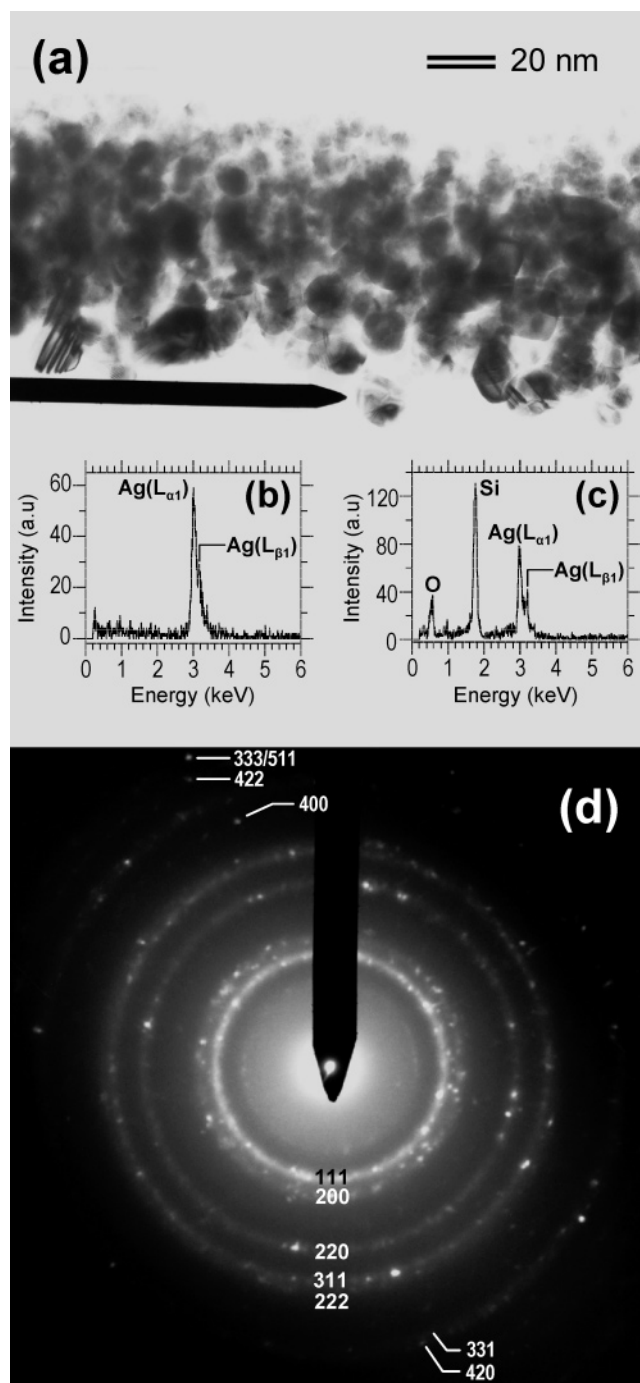


Figure 4. (a) TEM image of a Si nanocolumn coated with Ag nanoparticles. The column was removed from a 200 nm thick nanostructured c-v Si film that was immersed in 0.002 M AgNO_3 for 90 s with 20 rpm stirring at 20 °C for particle synthesis. (b) EDS signal sampled from the single Ag nanoparticle, which is pointed out by the beam stopper in part a. (c) EDS signal obtained from the center of the column shown in part a. (d) SAED pattern with indexed diffraction rings (characteristic of face-centered-cubic silver) obtained from a collection of Ag nanoparticles predominantly located at the lower edge of the column shown in part a. The sampled area is a 70 nm diameter circle, whose center is at the tip of the beam stopper.

nanoparticles surrounding the Si column are seen to be ~ 15 nm on the average. The nanoparticles appear overlapped especially in the middle region, since the electron beam is being transmitted through multiple Si and Ag nanocrystals situated across the column thickness. The Ag nanoparticles are distinguishable by their faceting as well as stacking faults and twins, which are not observed for Si nanoparticles building up the

nanocolumns for the magnification of Figure 4a.¹³ Furthermore, single Ag nanoparticles are distinguishable in Figure 4a as they protrude from the column. In fact, when we carried out EDS on one such single nanoparticle, which is pointed with the beam stopper in Figure 4a, two characteristic Ag peaks ($L_{\alpha 1}$ 2.98 keV and $L_{\beta 1}$ 3.15 keV) were observed in the EDS signal, whereas no Si was detectable (Figure 4b). When the same electron beam was focused in the middle of the column, the characteristic Si peak at 1.74 keV was found to dominate the EDS signal as shown in Figure 4c. The Si peak is also accompanied by the O peak (0.53 keV) indicative of the oxidation of Si at the expense of its reducing Ag^+ . The selective area electron diffraction (SAED) pattern shown in Figure 4d was obtained from an area of ~ 70 nm diameter centered at the point indicated by the tip of the beam stopper. Hence the electron diffraction signal was predominantly collected from the Ag nanoparticles at the edge of the column of Figure 4a. The diffraction rings are indexed to face-centered-cubic silver, with a lattice constant of 4.08 Å. For convenience, the innermost ring, which corresponds to (111) planes of the Si nanocrystals, was not indexed in Figure 4d. This diffraction ring as well as others consistent with the diamond structure of Si (i.e., corresponding to (111), (220), (311) planes) became very prominent when the same electron beam is focused at the center of the column of Figure 4a (not shown in this report). In summary, our TEM and EDS data provide further evidence that the Ag nanoparticles are synthesized and immobilized at the lateral surfaces of the Si columns by our process. The Ag nanoparticles exhibit irregular shapes and faceting although the majority could be considered roughly spherical or ellipsoidal. Twins or stacking faults are clearly visible in some of these Ag nanoparticles.

For particle sizes ≤ 20 nm, which is \ll the characteristic plasma excitation wavelength (e.g., ~ 400 nm), the plasma oscillations are not subject to phase retardation (quasi-static regime).^{5,22} Consequently, the plasmon decay occurs only nonradiatively and there is no scattering (which starts to dominate for particle sizes ≥ 30 nm).^{5,22} Furthermore, for this size range, plasmon modes higher than the dipolar are negligible. As a result, optical extinction essentially equals dipolar plasma absorption, which is proportional to particle volume.^{5,22} Since the sum of individual nanoparticle's extinction cross sections accounts for the extinction coefficient (Beer–Lambert law, in the case of insignificant electromagnetic coupling between particles), the extinction coefficient is proportional to the total volume of Ag particles synthesized. As seen from the inset of Figure 4a, at growth saturation, the Ag nanoparticles at the top of the Si film exhibit a narrow size distribution centered around 20 nm (i.e., the peak and the average) with the sizes of 93% of the particles falling ≤ 24 nm. Furthermore, out of hundreds of nanoparticles imaged in the void network of the c-v Si film by SEM and TEM only a few were found to exceed 20 nm in size. Therefore, the particle distribution observed does not only confirm the particle size control aspect of our approach, but it also suggests that, on the basis of above discussion, the optical extinction should approximately scale with the total particle volume during synthesis. Accordingly, we have monitored total Ag volume and, therefore the kinetics of Ag nanoparticle growth on our nanostructured Si film by following the time evolution of plasmon extinction at 400 nm. The plasmon extinction was simply obtained by subtracting the optical extinction due to the c-v Si film from total optical extinction (c-v Si film + Ag particles) as discussed in the Experimental Section.

The Ag growth kinetics was found to be the same with Ag_2SO_4 and AgNO_3 as long as the Ag^+ concentrations were equal.

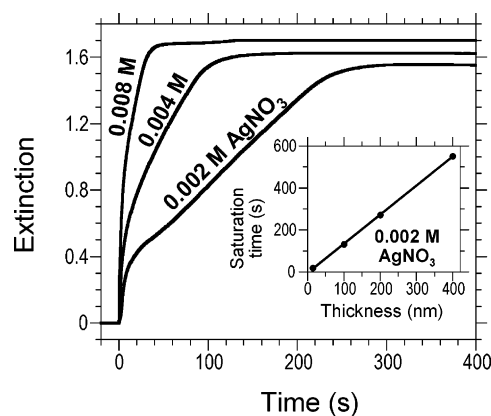


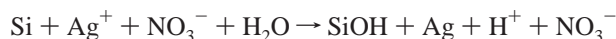
Figure 5. Kinetics of Ag nanoparticle synthesis as monitored from plasmon extinction (at 400 nm) for various AgNO_3 concentrations at 20 °C without stirring. The film thickness is 200 nm. The inset shows the dependence of saturation time on film thickness for 0.002 M AgNO_3 .

Figure 5 specifically shows the time evolution of the plasmon extinction (at 400 nm) for a c-v Si film thickness of ~ 200 nm and various concentrations of AgNO_3 . Obviously, the nanoparticle synthesis is self-limiting as evidenced by the saturation of the extinction. Although the kinetics is faster at higher concentrations, the saturated extinction values are very close for the concentrations examined. Earlier work on electroless metal depositions on semiconductors established nucleation occurs at “active” or “specific” sites on the surface such as steps, kinks, or other surface defects.^{16–18} Hence, final nanoparticle density is expected to have a weak dependence on concentration, if any. Accordingly, the slight increase of extinction (i.e., Ag volume) with solution concentration could arise from increased average particle size. Although we have not yet investigated how particle size correlates with solution concentration, in ref 19 it is reported that the size of the Ag nanostructures deposited on Si nanowires increases with solution concentration.

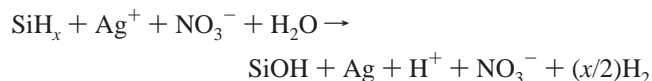
An interesting feature of the kinetics of Figure 5 is its linear regime, where extinction increases at almost a constant rate with time. Additionally, this regime is found to shorten with decreasing film thickness accounting for a shortened saturation time down to 20 s as shown in the inset of Figure 5. Furthermore, as deduced from the extinction spectra of Figure 2, the plasmon peak does not shift at all during this regime, and its fwhm only increases by 10%. Therefore, this linear regime of Figure 5 cannot be associated with a situation where all the nanoparticles grow simultaneously from a few nanometers (nucleation) to their maximum size of ~ 20 nm. If that were the case, the shape and position of the plasmon band would show more dramatic changes.⁵ We explain these observations as follows: When a Si film is immersed in an Ag^+ solution, the growth is expected to initiate simultaneously everywhere throughout the thickness of the film. However, the Ag^+ ions down inside the void volume are probably quickly depleted, before significant growth takes place. Then, at these depths in the c-v Si film the growth becomes limited by the transport of Ag^+ from outside. Therefore, the significant growth effectively follows an Ag^+ concentration front diffusing into the voids from top to bottom. This Ag^+ penetration front moves relatively slowly, because Ag^+ is being consumed by the nanoparticle synthesis. This subsequent “layer-by-layer” growth of nanoparticles from top to bottom corresponds to the steady growth rate regime seen in Figure 5. For this linear regime, a systematic increase of the growth rate (i.e., slope) with Ag^+ concentration is observed; i.e., from 0.0052 to 0.010 to 0.023 1/s as the AgNO_3

concentration is varied from 0.002 to 0.004 to 0.008 M, respectively. The linear dependence of the growth rate on concentration (i.e., concentration gradient) is consistent with a diffusion controlled growth mechanism. We argue that, prior to the linear regime the synthesis mainly proceeds by consuming the Ag^+ already present in the void volume, which means a larger volume of Ag synthesized (i.e., higher optical extinction) at the onset of the linear regime for higher Ag^+ concentrations. This is actually what we see in Figure 5. In addition to the Ag^+ concentration and film thickness, another parameter influencing the kinetics (i.e., saturation time) was found to be motion of the solution with respect to the Si film. For instance, the saturation time encountered in Figure 2 is ~ 90 s when the synthesis involved solution stirring (20 rpm) in a standard 400 mL beaker. On the other hand, as seen from Figure 5, when a corresponding film of $2/3$ the thickness is placed in a still 3.5 mL cell, the saturation time is seen to be much longer (270 s) for the same Ag^+ concentration of 0.002 M (despite the lower thickness). We attribute the shorter saturation time in the case of stirring to enhanced supply of Ag^+ to the film surface (entrance of voids) providing a higher concentration gradient and, therefore, a higher diffusion flux of Ag^+ through the voids.

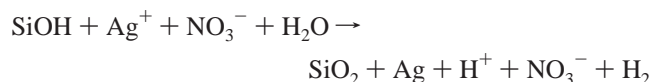
While the limited Ag^+ transport down into the void network accounts for the progressive layer-by-layer mode of growth in the voids, there must be an inhibiting mechanism that actually stops the synthesis, as is observed. We believe this mechanism is the blockage of the Si electron replenishment by the oxide growing on the Si surface during Ag synthesis. The re-supply of electrons is essential for the continuation of the Ag growth because there must be compensation for the Si electrons lost through reducing Ag^+ . The replenishing ($-$) charge to Si is provided by OH^- , which is created in parallel with the production of the H^+ replacing Ag^+ , through dissociation of H_2O . The net reaction may be given as:



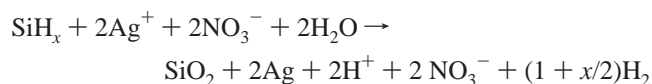
Here, the Si would be a surface atom bonded to neighboring Si atoms with one or more remaining dangling bond(s); e.g., $\equiv\text{Si}^\cdot$, $=\text{Si}^\cdot$. As will be discussed in the IR spectroscopy section of this article, such surface atoms are most likely to be passivated by H, given our c-v Si film preparation technique. Hence, the starting c-v Si is expected to be covered with SiH_x , and consequently the reaction above may be generalized to:



Reduction–oxidation can further proceed to yield SiO_2 as:



Or, the overall reduction–oxidation may be shown as:



For AgNO_3 concentrations higher than 0.01 M, bubbling is clearly observed during the reaction, which we attribute to H_2 formation in agreement with ref 19. In our c-v material, as well as in other nanostructured Si, it is likely that temporary charging during chemical reactions (e.g., $\text{Si} \rightarrow \text{Si}^+ + \text{e}^-$) induces high electric fields at high curvature features (i.e., at the nanoscale).

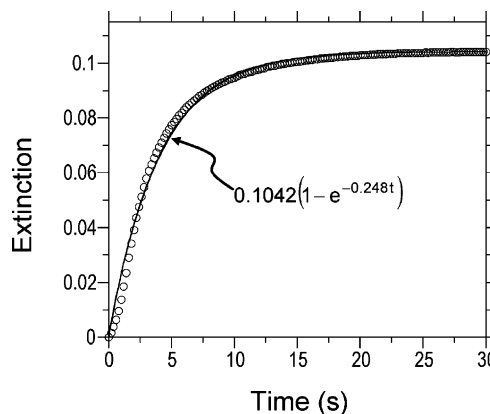


Figure 6. Time evolution of the plasmon extinction (at 400 nm) associated with Ag nanoparticles being synthesized when a ~ 20 nm thick nanostructured Si film is immersed in 0.0005 M AgNO_3 with no stirring at 20 °C. The solid line is the theoretical fit to the measured data (circles) representative of the kinetics of the formation of a Ag nanoparticle monolayer.

These enhanced fields facilitate charge/ion transport through the oxide layer and enable the reduction–oxidation reactions to take place to a larger extent permitting the formation of stable nanoparticles without the need for oxide removal by HF.

While OH^- functions as an electron supplier for Si it also acts as a precursor for its oxidation. However, the latter mechanism impedes and inhibits the former rendering the overall synthesis self-inhibiting. This self-inhibiting aspect of the growth is the key to nanoparticle size control seen with our c-v Si. The transport of the reducing electrons from Si to Ag^+ is anticipated not to be impeded by the oxide as these electrons can easily be conducted through Si to the Ag nanoparticle/solution interface, where they reduce the Ag^+ ions. Therefore, by virtue of silicon's being a semiconductor, oxidation and the Ag^+ reduction do not have to occur at the same location. In fact, refs 16 and 18 show evidence obtained by SEM and X-ray photoelectron spectroscopy (XPS) that the oxidation occurs alongside rather than beneath the nanoparticles. Nevertheless, whether oxide impedes and inhibits the transfer of reducing electrons to the Ag^+ , the transfer of the replenishing ($-$) charge to the Si, or both, it will have the same impact on the kinetics.

With the objective of elucidating this inhibiting mechanism and isolating it from the Ag^+ transport, we studied the kinetics with ultrathin films as seen in Figure 6. Here, a c-v Si film thickness of ~ 20 nm was used, which should allow the formation of only a monolayer (2D ensemble) of Ag particles. Since all these particles are situated at or very close to the external surface of the film (i.e., to the Ag^+ reservoir), the growth should not be limited by Ag^+ diffusion. Because of the charge balance, the final amount of Ag to be synthesized, V_∞ , must scale with the final amount of oxidized Si. Similarly, the number of Si atoms, which have been oxidized at some time t , should scale with $V(t)$, the volume of Ag produced by time t . Following Fujimura et al.²³ and Neuwald et al.²⁴ we assume that the oxidizing Si regions undergo this step stochastically. In particular, Fujimura et al. have inferred from infrared spectroscopy that native oxide growth on H-terminated Si (in H_2O) occurs randomly and insularly rather than through a layer-by-layer mechanism.²³ Similarly, Neuwald et al.'s SEM investigation of native oxide growth on H-terminated Si (in moist air) has shown that oxidation proceeded with the continuous formation of 2D oxide clusters, which did not grow larger than 10–20 Å in diameter.²⁴ The oxidation was found to be dominated by formation of additional nuclei, randomly distrib-

uted over the flat terraces. Accordingly, it is a valid assumption that in our case the Si regions are involved in oxidation in a stochastic way, as well. Therefore, in the regime where the Si oxide formation controls oxidation–reduction, the neutral Ag production rate should simply be proportional to the amount of Si left to oxidize; i.e., $\dot{V}(t) \propto (V_\infty - V(t))$, which is solved to give $V(t) = V_\infty(1 - e^{-at})$. Here a is the time constant. As noted, nanoparticle synthesis on the ultrathin film of Figure 6 should only be rate limited by oxidation. Hence, the kinetics data for this film should be a benchmark for the above model. As seen in Figure 6, the agreement between the data and model is good. The small discrepancy at the initiation of growth arises from the simplification in the model that nucleation of Ag is instantaneous, whereas the “concave up” feature of the kinetics up to ~ 2 s implies simultaneous nucleation and growth that, however, lasts for a very short period.^{17,18} The use of relatively low AgNO_3 concentration in Figure 6 (0.0005 M) is meant to slow the kinetics, so that more data could be sampled at the initial stage of synthesis, where growth occurs at the maximum rate. This also ensures the filling of the quartz cell with AgNO_3 takes place in a sufficiently short period (i.e., instantly) within the time scale of synthesis. Nevertheless, data sampled for higher AgNO_3 concentrations of 0.001 and 0.002 M were also found to fit well to $V(t) = V_\infty(1 - e^{-at})$.

For films which are not ultrathin so that multiple layers of nanoparticles are synthesized at different depths in the void network, we earlier argued for a progressive mode of growth from top to bottom. If a given monolayer at some depth in the voids effectively starts growing with a time lag of δ after the layer above it (i.e., following the Ag^+ front), then the total reduced Ag $V_{\text{total}}(t)$, at time t , will be the sum of contributions from individual monolayers; i.e., $V_{\text{total}}(t) = V(t) + V(t - \delta) + V(t - 2\delta) + \dots + V(0)$. Or, $V_{\text{total}}(t) \propto \sum_{\Delta t = 0, \delta, 2\delta, 3\delta, \dots, \min(t, t_{\text{saturation}})} (1 - e^{-a(t - \Delta t)})$. When this sum is computed including 10 or more terms, i.e., $\delta \leq t/10$, it predicts the constant growth rate regime of Figure 5 very well. This can also be seen if the sum is approximated with integration, i.e., $V_{\text{total}}(t) \approx K \int_{\Delta t=0}^t (1 - e^{-a(t - \Delta t)}) d\Delta t = Kt + (K/a)(e^{-at} - 1)$, where K is an appropriate constant. It is clear that the growth rate becomes constant once the exponential term decays. Therefore, the constant growth rate is a consequence of the growth front moving at a constant speed from top to bottom.

In an attempt to shed further light on the nanoparticle synthesis and simultaneous oxidation of Si, we probed the surface chemistry changes during particle growth with infrared (IR) spectroscopy. The IR absorption spectra of a c-v Si film before and after particle synthesis (i.e., 110 s of 0.002 M AgNO_3 immersion) are compared in Figure 7. As seen, the as-deposited c-v Si film exhibits the same Si–H infrared-active vibrational modes encountered in hydrogenated microcrystalline Si ($\mu\text{c-Si:H}$) films obtained by H_2/SiH_4 plasmas.²⁵ It is well established that in $\mu\text{c-Si:H}$, H passivates the Si dangling bond sites, which are predominantly located at the external surface and grain boundaries.²⁵ The 2100 cm^{-1} band is assigned to the Si–H stretching mode associated with dihydride groups, $=\text{SiH}_2$, or polymeric-like arrangements, $(\text{SiH}_2)_n$. The Si–H bending modes at 905 and 858 cm^{-1} are also indicative of $=\text{SiH}_2$ groups or $(\text{SiH}_2)_n$ arrangements which are seen to disappear upon Ag synthesis. The integrated intensity of the Si–H wagging band at 640 cm^{-1} is commonly used to quantify H-content as it is ascribed to all types of SiH_n ($n = 1, 2, 3$) arrangements. Although H terminating the Si surface is expected to be knocked off by oxidation, the wagging and stretching modes are seen to persist at a significant level after oxidation has occurred. Hence,

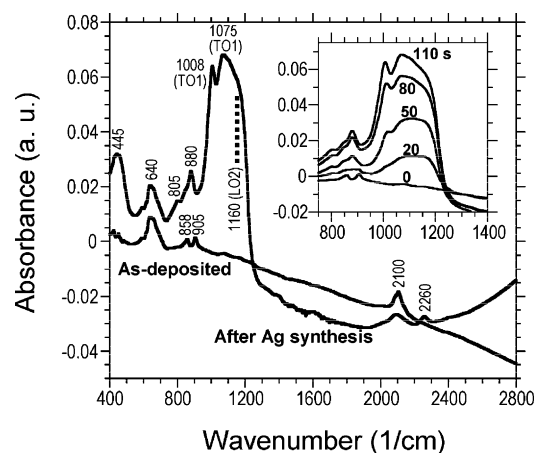


Figure 7. The IR absorption spectra of a 300 nm thick nanostructured c-v Si film before and after Ag nanoparticle synthesis (i.e., immersion in 0.002 M AgNO_3 , 110 s, 20 °C, 20 rpm stirring). The inset depicts the systematic increase of the Si–O–Si stretching band during Ag synthesis.

we infer a major fraction of H is present at the grain boundaries of Si nanocrystals, which are the building blocks of the columns. We observe the same result if we immerse our c-v Si films in H_2O_2 (30%, 10 min, 20 °C).¹³ Upon immersion in AgNO_3 , oxidation of Si takes place in parallel with Ag synthesis as evidenced in the IR data from the emergence of the prominent Si–O–Si bond-stretching mode exhibiting double peaks at 1075 and 1008 cm^{-1} . Although both of these vibrations are associated with the $=\text{Si-O-Si}=$ linking units, the frequency difference arises from the difference in host matrix (polarization) that surrounds the units as well as the variation in Si–O–Si angle.^{26,27} The Si–O–Si bond-stretching frequency has been known to increase monotonically with the $[\text{O}]/[\text{Si}]$ ratio. For example, it shifts from 940 cm^{-1} in O-doped amorphous Si to $\sim 1000\text{ cm}^{-1}$ in SiO and to 1075 cm^{-1} in stoichiometric amorphous SiO_2 .^{26–28} Accordingly, the Si–O–Si stretching peaks seen in Figure 7 at 1075 and 1008 cm^{-1} indicate that the oxidation of Si (driven by the reduction of Ag^+) predominantly results in SiO_2 and $\text{SiO}_{x \approx 1}$ domains, respectively. Sun et al. have employed XPS to observe suboxide growth on Si nanowires during the reduction of Ag^+ .¹⁹ The intensity of their O-shifted XPS Si peaks (2s and 2p) was found to slowly increase with the Ag^+ concentration. This implies a slow increase of synthesized Ag volume with $[\text{Ag}^+]$, which we see directly from our Figure 5.

The 1075 cm^{-1} peak, which is the transverse optical “in phase” antisymmetric Si–O–Si stretching mode (TO1),^{29,30} can broaden with disorder in addition to its lower energy shift with $[\text{Si}]/[\text{O}]$ ratio.^{26–28} However, disorder cannot alone account for this mode’s broadening toward higher energies to the extent seen in Figure 7.^{26–28} In fact, the shape of the stretching band at the higher energy side suggests the presence of an unresolved peak. In light of the literature, we ascribe this new mode to the longitudinal optical “out of phase” antisymmetric Si–O–Si stretching vibration (LO2) located at 1160 cm^{-1} .^{29,30} LO2 is excited and pronounced in ultrathin oxide films under two conditions: oblique incidence (Berreman effect) and disorder.^{29,30} Our IR characterization involved normal incidence to the substrate, which therefore was aligned at glancing angles to the lateral surface of the Si columns. Reports on electrochemically³¹ and stain-etched³² porous Si films clearly show the emergence of a peak at $\sim 1160\text{ cm}^{-1}$ upon oxidation whose origin was not discussed, but which we think is most likely the LO2 mode. Furthermore, we observe that this $\sim 1160\text{ cm}^{-1}$ peak

is the dominant peak in the IR spectrum when our c-v Si films are immersed in 30% H₂O₂ for 10 min at room temperature.¹³

The inset of Figure 7 depicts a systematic increase of the Si—O—Si stretching intensity during Ag synthesis for the same Ag⁺ concentration, stirring rate, and film thickness as in Figure 2. Comparison with Figure 2 reveals that the amounts of oxide and Ag synthesized follow the same trend simultaneously: a monotonic increase up to 80–90 s, beyond which saturation occurs. This supports the picture that Si reduces Ag⁺ at the expense of its being oxidized. Accordingly, Ag nanoparticle synthesis occurs by Si substrate reduction for our films and not by autocatalysis or substrate (Si) catalysis.^{17,18}

In Figure 7, oxidation also manifests itself with the peaks appearing at 805 and 445 cm⁻¹ assigned to Si—O—Si bending and rocking modes, respectively.^{29,30} Emergence of two new modes at 2260 and 880 cm⁻¹ upon Ag particle synthesis is also seen. These modes are ascribed to Si—H stretching and bending associated with $\equiv(3\cdot\text{O})\equiv\text{Si}-\text{H}$ groups, 3 O atoms being backbonded to Si.³³ The $\equiv(3\cdot\text{O})\equiv\text{Si}-\text{H}$ groups form in suboxides when Si has to bond to 3 O instead of 4, and the resulting dangling bond is passivated by H. Therefore, the oxide produced on our film during Ag nanoparticle growth is inferred to be highly disordered and hydrogenated, and to include both stoichiometric and suboxide domains.

Conclusions

In conclusion, deposited nanostructured column-void Si was demonstrated to reduce silver metal salts and lead to the synthesis of monodispersed, immobilized, and size-controlled Ag nanoparticle ensembles. The present article adopted Ag nanoparticles as the focus of interest due to their superior coupling with light (e.g., highest SERS gains), but we have also successfully extended the technique to the synthesis of Au, Pd, and Pt nanoparticles. An attractive aspect of our approach is that no surfactant, capping, or linking agents are needed for aggregation control, size control, and immobilization. In the case of surface-enhanced molecular detection, the absence of any surfactant or capping agent on the nanoparticle surfaces is a substantial benefit. It is ideal for analyte adsorption and eliminates background signals due to such agents. In addition, the ability to obtain monodispersed metal nanoparticles on any substrate using coatings of our reducer films further increases the effectiveness of our approach for various surface-enhanced analytical techniques.

In our c-v material, as well as in other nanostructured Si, it is likely that the enhanced electric fields at high curvature features (i.e., at the nanoscale) facilitate charge transport through the oxide layer permitting the formation of stable nanoparticles without the need for oxide removal by HF. We believe the unique, systematically varying topography, and therefore systematically varying field regions, of the c-v Si result in monodispersion of the synthesized nanoparticles. The immobilization results from a combination of steric hindrance and enhanced induced dipole–dipole attractions due to the nanoscale topography while, as we deduce from kinetics and surface chemistry changes, the nanoparticle size control is principally due to the role of the oxide in self-inhibiting synthesis. These unique features of monodispersion, immobilization, and size

control are lost when flat Ge (with an aqueous solution) or flat Si (with HF) substrates are used as the reducer.^{14,18}

Acknowledgment. This research was supported in part by the National Science Foundation (Grant No. DMI-0210229) and was performed using the facilities of the Penn State NSF National Nanofabrication Infrastructure Network (NNIN) site.

References and Notes

- (1) Nie, S.; Emory, S. R. *Science* **1997**, 275, 1102.
- (2) Kneipp, K.; Wang, Y.; Kneipp, H.; Perelman, L. T.; Itzkan, I.; Dasari, R. R.; Feld, M. S. *Phys. Rev. Lett.* **1997**, 78, 1667.
- (3) Haes, A. J.; Hall, W. P.; Chang, L.; Klein, W. L.; Van Duyne, R. P. *Nano Lett.* **2004**, 4, 1029.
- (4) Parfenov, A.; Gryczynski, I.; Malicka, J.; Geddes, C. D.; Lakowicz, J. R. *J. Phys. Chem. B* **2003**, 107, 8829.
- (5) Kreibitz, U.; Vollmer, M. *Optical Properties of Metal Clusters*; Springer: New York, 1995.
- (6) Malynych, S.; Luzinov, I.; Chumanov, G. *J. Phys. Chem. B* **2002**, 106, 1280.
- (7) Freeman, R. G.; Grabar, K. C.; Allison, K. J.; Bright, R. M.; Davis, J. A.; Guthrie, A. P.; Hommer, M. B.; Jackson, M. A.; Smith, P. C.; Walter, D. G.; Natan, M. J. *Science* **1995**, 267, 1629.
- (8) Yamanoi, Y.; Yonezawa, T.; Shirahata, N.; Nishihara, H. *Langmuir* **2004**, 20, 1054.
- (9) Lu, Y.; Liu, G. L.; Lee, L. P. *Nano Lett.* **2005**, 5, 5.
- (10) Chandrasekharan, N.; Kamat, P. V. *Nano Lett.* **2001**, 1, 67.
- (11) Fukuoka, A.; Araki, H.; Sakamoto, Y.; Sugimoto, N.; Tsukada, H.; Kumai, Y.; Akimoto, Y.; Ichikawa, M. *Nano Lett.* **2002**, 2, 793.
- (12) Kalkan, A. K.; Bae, S.; Li, H.; Hayes, D. J.; Fonash, S. J. *J. Appl. Phys.* **2000**, 88, 555.
- (13) Kalkan, A. K.; Henry, M. R.; Li, H.; Cuiffi, J. D.; Hayes, D. J.; Palmer, C.; Fonash, S. J. *Nanotechnology* **2005**, 16, 1383.
- (14) The authors have investigated Ag nanoparticle synthesis with nonporous flat microcrystalline and amorphous Si films. The synthesis was detectable by optical transmission only in the presence of HF. The plasmon optical extinction of the Ag nanoparticles synthesized in this case shows multiple resonances indicative of nanoparticle aggregates and larger particles (i.e., no particle size control).
- (15) Ohmi, T.; Imaoka, T.; Sugiyama, I.; Kezuka, T. *J. Electrochem. Soc.* **1992**, 139, 3317.
- (16) Nagahara, L. A.; Ohmori, T.; Hashimoto, K.; Fujishima, A. *J. Vac. Sci. Technol. A* **1993**, 11, 763.
- (17) Oskam, G.; Long, J. G.; Natarajan, A.; Searson, P. C. *J. Phys. D: Appl. Phys.* **1998**, 31, 1927.
- (18) Porter, L. A.; Choi, H. C.; Ribbe, A. E.; Buriak, J. M. *Nano Lett.* **2002**, 2, 1067.
- (19) Sun, X. H.; Peng, H. Y.; Tang, Y. H.; Shi, W. S.; Wong, N. B.; Lee, C. S.; Lee, S. T.; Sham, T. K. *J. Appl. Phys.* **2001**, 89, 6396.
- (20) Coulthard, I.; Sham, T. K. *Solid State Commun.* **1998**, 105, 751.
- (21) Kalkan, A. K.; Li, H.; O'Brien, C. J.; Fonash, S. J. *IEEE Electron Device Lett.* **2004**, 25, 526.
- (22) Kreibitz, U.; Schmitz, B.; Breuer, H. D. *Phys. Rev. B* **1987**, 36, 5027.
- (23) Fujimura, S.; Ishikawa, K.; Ogawa, H. *J. Vac. Sci. Technol. A* **1998**, 16, 375.
- (24) Neuwald, U.; Hessel, H. E.; Feltz, A.; Memmert, U.; Behm, R. J. *Appl. Phys. Lett.* **1992**, 60, 1307.
- (25) Kroll, U.; Meier, J.; Shah, A.; Mikhailov, S.; Weber, J. *J. Appl. Phys.* **1996**, 80, 4971.
- (26) Lucovsky, G. *Solid State Commun.* **1979**, 29, 571.
- (27) Pai, P. G.; Chao, S. S.; Takagi, Y.; Lucovsky, G. *J. Vac. Sci. Technol. A* **1986**, 4, 689.
- (28) Weldon, M. K.; Stefanov, B. B.; Raghavachari, K.; Chabal, Y. J. *Phys. Rev. Lett.* **1997**, 79, 2851.
- (29) Kirk, C. T. *Phys. Rev. B* **1988**, 38, 1255.
- (30) Lange, P. *J. Appl. Phys.* **1989**, 66, 201.
- (31) Sasaki, Y.; Kitahara, M. *J. Appl. Phys.* **1994**, 76, 4344.
- (32) Jia, Y. Q.; Zhang, L. Z.; Fu, J. S.; Zhang, B. R.; Mao, J. C.; Qin, G. G. *J. Appl. Phys.* **1993**, 74, 7615.
- (33) Tsu, D. V.; Lucovsky, G.; Davidson, B. N. *Phys. Rev. B* **1989**, 40, 1795.